Parasitology Research (2019) 118:1533–1548
https://doi.org/10.1007/s00436-019-06206-z

IMMUNOLOGY AND HOST-PARASITE INTERACTIONS - ORIGINAL PAPER

In vitro evaluation of arylsubstituted imidazoles derivatives as antiprotozoal agents and docking studies on sterol 14α-demethylase (CYP51) from *Trypanosoma cruzi*, *Leishmania infantum*, and *Trypanosoma brucei*

Julio Alberto Rojas Vargas[1] · América García López[1] · Yulier Pérez[1] · Paul Cos[2] · Matheus Froeyen[3]

Received: 25 April 2018 / Accepted: 4 January 2019 / Published online: 23 March 2019

Abstract

There is an urgent need to discover and develop new drugs to combat parasitic diseases as Chagas disease (*Trypanosoma cruzi*), sleeping sickness (*Trypanosoma brucei*), and leishmaniasis (*Leishmania* ssp.). These diseases are considered among the 13 most unattended diseases worldwide according to the WHO. In the present work, the synthesis of 14 arylsubstituted imidazoles and its molecular docking onto sterol 14α-demethylase (CYP51) was executed. In addition, the compounds, antiprotozoal activity against *T. brucei*, *T. cruzi*, *Trypanosoma brucei rhodesiense*, and *Leishmania infantum* was evaluated. In vitro antiparasitic results of the arylsubstituted imidazoles against *T. brucei*, *T. cruzi*, *T.b. rhodesiense*, and *L. infantum* indicated that all samples from arylsubstituted imidazole compounds presented interesting antiparasitic activity to various extent. The ligands **5a**, **5c**, **5e**, **5f**, **5g**, **5i**, and **5j** exhibited strong activity against *T. brucei*, *T. cruzi*, *T.b. rhodesiense*, and *L. infantum* with IC_{50} values ranging from 0.86 to 10.23 μM. Most samples were cytotoxic against MRC-5 cell lines ($1.12 < CC_{50} < 51.09$ μM) and only ligand **5c** showed a good selectivity against all tested parasites. According to the results of the molecular docking, the aromatic substituents in positions 1, 4, and 5 have mainly stabilizing hydrophobic interactions with the enzyme matrix, while the oxygen from NO_2, SO_3H, and OH groups interacts with the Fe^{2+} ion of the Heme group.

Keywords Arylsusbtituted imidazoles · *Trypanosoma cruzi* · *Trypanosoma brucei* · *Trypanosoma b. rhodesiense* · *Leishmania infantum* · In vitro evaluation · Molecular docking

Section Editor: Sarah Hendrickx

✉ Julio Alberto Rojas Vargas
jarojas@uo.edu.cu

América García López
america@uo.edu.cu

Paul Cos
paul.cos@uantwerpen.be

Matheus Froeyen
mathy.froeyen@rega.kuleuven.be

[1] Chemistry Department, Exact and Natural Science Faculty, Oriente University, Santiago de Cuba, Cuba

[2] Laboratory of Microbiology, Parasitology and Hygiene (LMPH), S7, Faculty of Pharmaceutical, Biomedical and Veterinary Sciences, University of Antwerp, Wilrijk, Belgium

[3] Medicinal Chemistry, Department of Pharmacy, Rega Institute, KU Leuven, Leuven, Belgium

Introduction

Trypanosomatidae form a family of unicellular eukaryotic parasites from the order *Kinetoplastida*, phylum *Euglenozoa*, supergroup *Excavates*. Many human pathogens possess a number of species of kinds *Leishmania* and *Trypanosoma*. The life cycles of these organisms turn out to be very complex, constantly moving between insects and mammalian hosts (Guedes da Silva et al. 2017; Lepesheva et al. 2015).

Leishmaniasis is a common disease in many continents, each year 20,000 to 30,000 deaths and almost 1 million of new cases are reported, arriving to report oneself around 12 million infected people (Lepesheva et al. 2015). It is caused by unicellular eukaryotic organisms from genus *Leishmania* (Trypanosomatidae family). Analogous to other protozoan parasites, *Leishmania* has a complex life cycle, transmitted via the bite of female phlebotomine sandflies. The parasite exist in two forms namely *promastigote* in sandfly and

amastigote in human macrophage (Bates 2007; Rodríguez et al. 2006). It is exhibited in three clinical form: visceral leishmaniasis (*Leishmania donovani*, *Leishmania infantum*/*Leishmania chagasi*), also known as kala-azar; cutaneous leishmaniasis caused by *Leishmania major*, *L. donovani*, *Leishmania tropica*, and *Leishmania aethiopica*; and mucocutaneous leishmaniasis caused by *Leishmania braziliensis*.

American trypanosomiasis, more known as Chagas disease, is usually transmitted by the bites of triatomine insects, also known as "kissing bugs." These insects or their feces carry the flagellate parasite *Trypanosoma cruzi* (*T. cruzi*) and can also contaminate foods such as fruits juices, resulting in foodborne. It is an endemic disease in Central and South America, a few cases occur occasionally in the southern USA. This disease has become a growing problem in non-endemic areas, where infections may not be recognized by many people, and where the few effective drugs may not be generally available (Lepesheva et al. 2015).

Human African trypanosomiasis, known commonly as sleeping sickness, is caused by infection with protozoans of the genus *Trypanosoma*. It is transmitted by their only vector tsetse fly (*Glossina* genus) bites, which have acquired their infection from human or other animals that contain in her organism other human parasites (WHO 2017). This disease has two clinical manifestations, *Trypanosoma brucei gambiense* (*T.b. gambiense*) and *Trypanosoma brucei rhodesiense* (*T.b. rhodesiense*). The *T.b. gambiense* causes a more chronic infection that is responsible for over 90% of cases, whereas *T.b. rhodesiense* causes an acute infection that is responsible for a smaller proportion of the overall human African trypanosomiasis disease burden. The disease develops rapidly and invades the central nervous system (WHO 2017).

The patient may exhibit some of the following symptoms: fevers, skin eruptions, irregular febrile episodes, headaches, malaise, exhaustion, anorexia, extreme thirst, muscle and joint pains, anemia, rash, coma, and ultimately death. Sleeping sickness is endemic in 36 Sub-Saharan African countries, with an 85% case reduction since year 2000 and less than 3000 cases in year 2015, a record low with around > 60 million people are at risk (WHO 2017).

Sterol 14α-demethylase (CYP51, EC.1.14.13.70) has been found as a vital target for the development of anti-fungal, anti-leishmania, anti-trypanosoma drugs and also for the design of cholesterol-lowering drugs. Crystal structures of protozoan sterol 14α-demethylases provide an opportunity for structure-directed development of such inhibitors. The enzyme is responsible for catalyzing the elimination of the alpha-methyl group of the sterol, which leads to the formation of cholesterol in vertebrates, the well-known ergosterol in fungi, and several ergosterol alkylated derivatives (phytosterol) for plants and protozoa (Buckner and Urbina 2012). The production of ergosterol in fungus and protozoa, unlike mammals, is lethal when it accumulates, affecting cytokinesis, stopping cell growth to cause death of the cell membrane (Roberts et al. 2003). Extensive work is performed already considering CYP51 as target. Silva et al. (Guedes da Silva et al. 2017) have analyzed the effectiveness of two classes of drugs using CYP51: **VNI** and **VFV**. Schel et al. (2016) have demonstrated the anti-fungal activity of **VT-1161** and **VT-1129**, among many other application reports with the use of CYP51 target (Singh et al. 2015; Anusha et al. 2015).

Here, we report the synthesis, in vitro antiprotozoal activity, and cytotoxicity of 14 arylsubstituted imidazoles, as well as its molecular docking onto sterol 14α-demethylase (CYP51). We have chosen the CYP51 target because all analyzed compounds possess the principal pharmacophore features of CYP51 inhibitors reported by Vita et al., where they state that an active compound must contain a heterocycle with a nitrogen able to interact with the Fe atom present in the Heme group and having two hydrophobic groups near to it (De Vita et al. 2016).

Materials and methods

General procedure for the synthesis of substituted imidazoles

The arylsubstituted imidazoles were obtained by reaction of aromatic aldehydes, primary amines, benzils, and ammonium acetate (Fig. 1) catalyzed by boric acid (Shelke et al. 2009). All reagents used had commercial grade. Melting points were determined in open capillaries using a Digital Melting Point apparatus WRS-2A. ^{1}H-NMR and ^{13}C-NMR spectra were recorded with a Bruker DRX-600 spectrometer obtained in DMSO-d_6 and MeOD solutions. The FT-IR spectra were recorded on a Shimadzu-FTIR Infrared spectrometer in KBr (ν_{max} in cm^{-1}). The reaction occurred at the maximum energy area in the reaction vessel, where was slightly lower than the level of the water and the temperature was controlled at 60 °C.

Reaction conditions are as follows: aldehyde **1** (1 mmol), amine **2** (1 mmol), ammonium acetate **3** (1.5 mmol), benzil **4** (1 mmol), H_3BO_3 (5 mol%), and propylene glycol (15 mL) heating under reflux for 6 h.

The products (**5a-n**) in Table 1 were confirmed by the analysis of spectra ^{1}H-NMR, ^{13}C-NMR, FT-IR, mass spectra, and the melting points obtained for each compounds.

Antiparasitic activity

All compounds were in vitro tested against *T. cruzi* Tulahuen CL2, β-galactosidase strain (nifurtimox-sensitive), *L. infantum* (MHOM/MABE/67 amastigotes), and *T. brucei* (Squib-427 strain, suramin-sensitive) and *T.b. rhodesiense* (strain STIB-900).

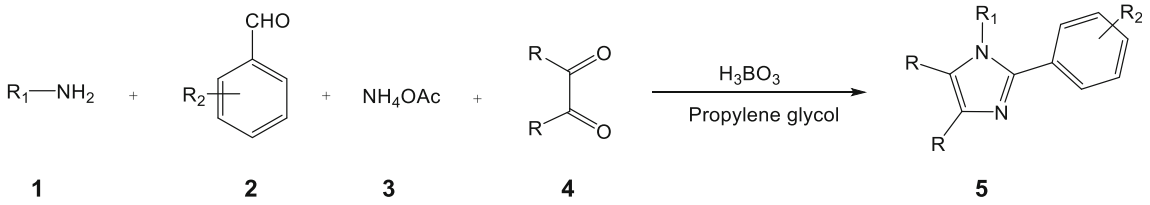

Fig. 1 Synthesis of arylsubstituted imidazoles

Compound stock solutions were prepared in DMSO at 20 mM. The compounds were serially pre-diluted (2-fold or 4-fold) in DMSO followed by a further (intermediate) dilution in demineralized water to assure a final in-test DMSO concentration of < 1%. Test plates are identical for all screens and produced as a single batch. The results were expressed as % reduction in parasite burdens compared to control wells and an IC_{50} (50% inhibitory concentration) was calculated. The in vitro screening was carried out according to the previously described procedure (Cos et al. 2006).

Trypanosoma cruzi, Tulahuen CL2, β-galactosidase strain (nifurtimox-sensitive) was used. The strain was maintained on MRC-5_{SV2} (human lung fibroblast) cells in MEM medium, supplemented with 200 mM L-glutamine, 16.5 mM $NaHCO_3$, and 5% inactivated fetal calf serum. All cultures and assays were conducted at 37 °C under an atmosphere of 5% CO_2. Assays were performed in sterile 96-well microtiter plates, each well containing 10 μl of the watery compound dilutions together with 190 μl of MRC-5 cell/parasite inoculum (2.10^4 cells/ml + 2.10^5 parasites/ml). Parasite growth was compared to untreated-infected controls (100% growth) and non-infected controls (0% growth) after 7 days incubation. Parasite burdens were assessed after adding the substrate CPRG (chlorophenol red β-D-galactopyranoside): 50 μl/well of a stock solution containing 15.2 mg CPRG + 250 μl Nonidet in 100 ml PBS. The change in color was measured at 540 nm after 4 h incubation at 37 °C. **Benznidazole** was included as reference drug. The test compound is classified as inactive when the IC_{50} is higher than 30 μM. When IC_{50} lies between 30 and 5 μM, the compound is regarded as being moderate active. When the IC_{50} is lower than 5 μM, the compound is classified as highly active on the condition that it also demonstrates selective action (absence of cytotoxicity).

Trypanosoma brucei brucei Squib 427 strain (**suramin**-sensitive) and *T.b. rhodesiense* (strain STIB-900) were used for screening. The strains are maintained in Hirumi (HMI-9) medium, supplemented with 10% inactivated fetal calf serum. All cultures and assays were conducted at 37 °C under an atmosphere of 5% CO_2. Assays were performed in sterile 96-well microtiter plates, each well containing 10 μl of the compound dilutions together with 190 μl of the parasite suspension (1.5×10^4 parasites/well—*T.b. brucei*, and 4×10^3 parasites/well—*T.b. rhodesiense*). Parasite growth was compared to untreated-infected (100% parasite growth) and uninfected controls (0% growth). After 3 days incubation, parasite growth was assessed fluorimetrically after addition of 50 ml resazurin per well. After 6 h (*T.b. rhodesiense*) or 24 h (*T.b. brucei*) at 37 °C, fluorescence was measured (λ_{ex} 550 nm, λ_{em} 590 nm). **Suramin** (*T.b. brucei* and *T.b. rhodesiense*) was included as the reference drugs. The compound is classified as inactive when the IC_{50} is higher than 5 μM. When IC_{50} lies between 5 and 1 μM, the compound is regarded as being moderate active. When the IC_{50} is lower than 1 μM, the compound is classified as highly active on the condition that it also demonstrates selective action (absence of cytotoxicity).

Leishmania infantum MHOM/MA(BE)/67 was maintained in the golden hamster (*Mesocricetus auratus*) and spleen amastigotes were collected for infection. Primary peritoneal mouse macrophages (PMM) were used as host cells and were collected 2 days after peritoneal stimulation with a 2% potato starch suspension. Assays were performed in 96-well microtiter plates, each well containing 10 μl of the compound dilutions together with 190 μl of macrophage-parasite inoculum (3.10^5 cells + 3.10^6 parasites/well // RPMI-1640 + 5% FCSi). After 5 days incubation, total amastigote burdens were microscopically assessed after Giemsa staining. **Miltefosine** was included as reference drug. A test compound is classified as inactive when the IC_{50} is higher than 30 μM. When IC_{50} lies between 30 and 10 μM, the compound is regarded as moderately active. If the IC_{50} is lower than 10 μM, the compound is

Table 1 Chemical structure of arylsubstituted imidazole

Entry	Compound	R	R	R_1	R_2
1	**5a**	Ph	Ph	Ph-CH_2	p-$N(CH_3)_2$
2	**5b**	Ph	Ph	Ph-CH_2	p-OH
3	**5c**	Ph	Ph	Ph-CH_2	H
4	**5d**	Ph	Ph	Ph-CH_2	p-OCH_3
5	**5e**	Ph	Ph	m-CH_3-C_6H_5-	m-NO_2
6	**5f**	Ph	Ph	o-CH_3-C_6H_5-	p-NO_2
7	**5g**	Ph	Ph	m-CH_3-C_6H_5-	p-NO_2
8	**5h**	Ph	Ph	p-CH_3-C_6H_5-	p-NO_2
9	**5i**	Ph	Ph	p-SO_3H-C_6H_5	p-$N(CH_3)_2$
10	**5j**	Ph	Ph	–	p-$N(CH_3)_2$
11	**5k**	Ph	Ph	Fu-CH_2	4-OH, 3-CH_3O
12	**5l**	Fu	Fu	–	4-OH, 3-CH_3O
13	**5m**	Fu	Fu	–	C_6H_5
14	**5n**	Fu	Fu	Fu-CH_2	p-OH-C_6H_5

Ph phenyl, *Fu* furyl

classified as highly active on the condition that it also demonstrates selective action (absence of cytotoxicity against primary peritoneal macrophages).

In vitro cytotoxicity evaluation on human fibroblasts (MRC-5 cell line)

MRC-5_{SV2} cells were cultured in MEM + Earl's salts-medium, supplemented with L-glutamine, $NaHCO_3$, and 5% inactivated fetal calf serum. All cultures and assays were conducted at 37 °C under an atmosphere of 5% CO_2. Assays were performed in 96-well microtiter plates, each well containing 10 μl of the watery compound dilutions together with 190 μl of MRC-5_{SV2} inoculum (1.5×10^5 cells/ml). Cell growth was compared to untreated-control wells (100% cell growth) and medium-control wells (0% cell growth). After 3 days incubation, cell viability was assessed fluorimetrically after addition of resazurin (λ_{ex} 550 nm, λ_{em} 590 nm). **Tamoxifen** was used as positive control. The compound is classified non-toxic when the IC_{50} is higher than 30 μM. Between 30 and 10 μM, the compound is regarded as moderately toxic. When the IC_{50} is lower than 10 μM, the compound is classified as highly toxic.

Molecular docking

Ligands and proteins preparation

Molecular modeling was performed using the high-performance computing capabilities of the Cluster of Chemistry Department of University of Oriente running the Linux operating system Debian 8.0 distribution. The pdb file was prepared using the software UCSF Chimera molecular graphic system, version 1.10.227 (Pettersen et al. 2004). Cytochrome P450 14α-sterol demethylase, CYP51, of the species *T. cruzi*, *T. brucei*, and *L. infantum* was selected: CYP51 of *T. cruzi* in complex with an inhibitor **VNF** ((4-(4-chlorophenyl)-N-[2-(1H-imidazol-1-yl)-1-phenylethyl]benzamide)—PDB ID: **3KSW** (*CYP51—T. cruzi*) (Lepesheva et al. 2010) with a resolution of 3.05 Å, CYP51 of *T. brucei* bound to (S)-N-(3-(1H-indol-3-yl)-1-oxo-1-(pyridin-4-ylamino)propan-2-yl)-3,3′-difluoro-(1,1′-biphenyl)-4-carboxamide—PDB ID: **4BJK** (*CYP51—T. brucei*) (Choi et al. 2013) with a resolution of 2.67 Å and CYP51 of *L. infantum* in complex with fluconazole—PDB ID: **3L4D** (*CYP51—L. infantum*) (Hargrove et al. 2011) with resolution of 2.75 Å. The structures **3L4D** and **4BJK** contained identical domains; we selected chain A for the docking experiments. Structure **3KSW** contained only one chain. Finally, the resulting prepared 3D structure of the proteins was saved as PDB file, using AutodockTools 1.5.6 (Sanner 1999).

Kollman united atom charges, solvation parameters, and polar hydrogens were added to the receptor. Since the ligands are not peptides, Gasteiger charges were assigned and non-polar hydrogens were merged. ChemBioDraw (Evans 2014) was used to draw and design the structures of arylsubstituted imidazoles (Fig. 1) taking into account reference Planche et al. (2009). ChemBio3D Ultra 12.0 (Evans 2014) was used to optimize the geometry, running a MMFF94 energy minimization of the 3D structures. The Gasteiger charge calculation method (Gasteiger and Marsili 1980) was used and partial charges were added to the ligand atoms prior to docking, via AutodockTools.

Identification of binding site residues

The binding site residues for *CYP51—T. cruzi, CYP51—T. brucei*, and *CYP51—L. infantum* were identified from the analysis of 3KSW, 4BJK, and 3L4D available in the RCSB Protein Data Bank. *CYP51—L. infantum* in the active site involves the amino acids Leu355, Met357, Leu358, Met459, Val212, Phe104, Met105, Tyr115, Ala114, Phe109, Gly282, Met283, Phe289, Leu129, Ala290, and Val460 (Hargrove et al. 2011), *CYP51—T. cruzi* involves the amino acids Tyr103, Met106, Phe110, Tyr116, Leu127, Ala297, Phe290, Ala291, Thr295, Leu356, Leu357, Met358, Met360, Val461, Met460, and Ala287 (Lepesheva et al. 2010), and *CYP51—T. brucei* involves the amino acids Tyr116, Tyr103, Met106, Phe105, Phe290, Ala287, and Phe110 (Choi et al. 2013) according to the references.

Grid box preparation and docking

Docking experiment were performed between arylsubstituted imidazoles and *CYP51—T. cruzi* and *CYP51—L. infantum* proteins. AutoDock requires pre-calculated grid maps, one for each atom type, present in the ligand being docked, as it stores the potential energy arising from the interaction with the macromolecule. This grid must surround the region of interest (active site) in the macromolecule.

Table 2 Grid box parameters selected for the target enzymes

Enzyme	x, y, z coordinates of left of box			Size (points)	Spacing (Å)
CYP51—T. cruzi	2.48	26.996	22.191	50 × 50 × 50	0.375
CYP51—L. infantum	31.917	− 28.96	− 1.658	50 × 50 × 50	0.375
CYP51—T. brucei	26.642	58.216	26.493	50 × 50 × 50	0.375

Grid box parameters (Table 2) were set by using AutoDockTools (ADT), a free graphic user interface of MGL software packages (version 1.5.6rc3) (Sanner 1999).

The molecular docking program AutoDock version 4.2 (Sanner 1999) was employed to perform the docking experiment. The Lamarckian Genetic Algorithm was used during the process to explore the best conformational space for the ligand with a population size of 50 individuals. The maximum number of generations and evaluations were set at 27,000 and 2,500,000, respectively. Other parameters were set as default. After complete execution of Autodock, 50 conformations of the ligands in complex with the receptor were obtained, which were ranked based on binding energy and inhibition constant (K_i).

To check the docking procedure and given the similar structure (imidazole and triazole rings) between the compounds here reported, we choose known CYP51 inhibitors, **VNF** ((R)-N-(2-(1H-imidazol-1-yl)-1-phenylethyl)-4′-chloro-[1,1′-biphenyl]-4-carboxamide) to *CYP51—T. cruzi* (Friggeri et al. 2014), ketoconazole (**KET**) for *CYP51—T. brucei* (Hargrove et al. 2012), and **VFV** ((R)-N-(1-(3,4′-difluorobiphenyl-4-yl)-2-(1H-imidazol-1-yl)ethyl)-4-(5-phenyl-1,3,4-oxadiazol-yl)benzamide) for *CYP51—L. infantum* (Lepesheva et al. 2015), which were rebuilt and redocked (Fig. 2).

Results and discussion

Synthesis and characterization of arylsubstituted imidazoles

Since arylsubstituted imidazoles have become increasingly useful and important in the pharmaceutical field, the development of clean, high-yielding, and environmentally friendly synthetic approaches is still desirable and much in demand. The synthesized imidazole derivatives were characterized after recrystallization from an appropriate solvent by recording their ^{1}H-NMR, ^{13}C-NMR, FT-IR, and MS spectra. The results of the synthesis are summarized in Table 3.

According to the results shown in Table 3, all synthesized compounds have a similar melting point and good yield compared with the reference.

Spectral data results

(**5a**) 4-(1-benzyl-4,5-diphenyl-1H-imidazol-2-yl)-N,N-dimethylaniline. **MW**: 429.57 **mp**: 151–153 °C (Reported: 150–152 °C (Kantevari et al. 2006)). **^{1}H-NMR** (600 MHz, DMSO-d_6): δ ppm 8.10–7.18 (m, 19H, Ar-H), 5,12 (s, 2H, CH_2), 3.34 (s, 6H, $CH_3 \times 2$). **^{13}C-NMR** (150 MHz, DMSO-d_6): δ ppm 155.2, 150.42, 141.3, 137.78, 131.51, 129.38, 128.94, 128.75, 128.60, 128.49, 128.35, 127.48, 126.38, 125.61, 118.42, 111.99(C_{arom}), 47.68 (CH_2), 41.02 (CH_3x2). **Mass spectrum (ES+)**. 430.23 $[M + H]^+$, 387.18, 340.18, 297.13.

(**5b**) 4-(1-benzyl-4,5-diphenyl-1H-imidazol-2-yl) phenol. **MW**: 402.49 **mp**: 136–139 °C (Reported: 135–138 (Khalafi-Nezhad et al. 2016)). **^{1}H-NMR** (600 MHz, DMSO-d_6): δ ppm 9.76 (s, 1H, OH), 6.74–7.46 (m, 19H), 5.11 (s, 2H, CH_2), **^{13}C-NMR** (150 MHz, DMSO-d_6): δ ppm 158.04, 153.84, 141.40, 137.57, 136.52, 134.75, 130.88, 130.07, 129.63, 128.80, 128.55, 128.10, 127.18, 126.10, 125.70, 121.57, 115.46 (C_{arom}), 47.63(CH_2). **Mass spectrum (ES+)**. 403.18 $[M + H]^+$, 313.13, 297.14.

(**5c**) 1-benzyl-2,4,5-triphenyl-1H-imidazole. **MW**: 386.50 **mp**: 158–160 °C (Reported: 155–158 (Khalafi-Nezhad et al. 2016)). **^{1}H-NMR** (600 MHz, DMSO-d_6): δ ppm 6.75–7.69 (m, 20H, Ar-H), 5,13 (s, 2H, CH_2). **^{13}C-NMR** (150 MHz,

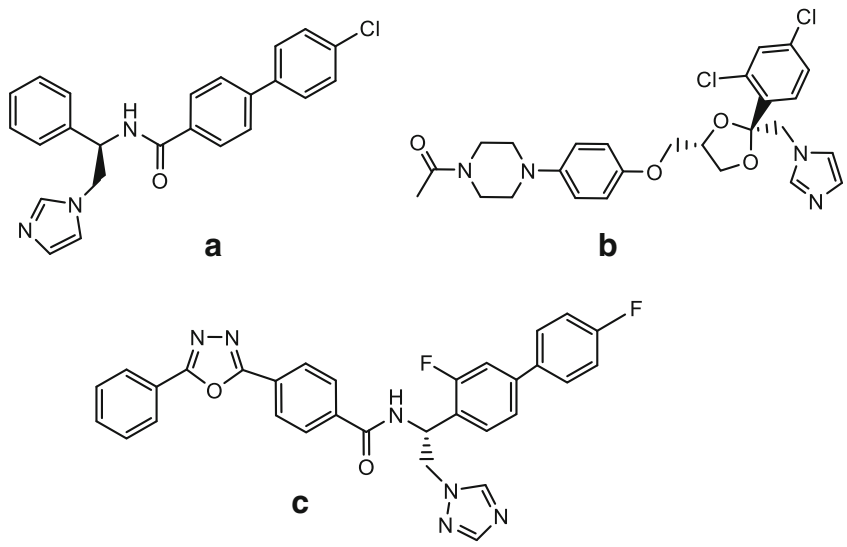

Fig. 2 Structure of control compounds **VNF** (**a**), **KET** (**b**), and **VFV** (**c**)

Table 3 Physical data and yields of arylsubstituted imidazoles

Product	R	R	R_1	R_2	Yield[a] (%)	M.P. (°C) (observed)	M.P. (°C) (literature)
5a	Ph	Ph	Ph-CH_2	p-$N(CH_3)_2$	89	151–153	150–152[b]
5b	Ph	Ph	Ph-CH_2	p-OH	88	136–139	135–138[c]
5c	Ph	Ph	Ph-CH_2	H	90	158–160	155–158[c]
5d	Ph	Ph	Ph-CH_2	p-OCH_3	91	165–168	167–169[c]
5e	Ph	Ph	m-CH_3-C_6H_5-	m-NO_2	89	165–166	–
5f	Ph	Ph	o-CH_3-C_6H_5-	p-NO_2	86	235–236	–
5g	Ph	Ph	m-CH_3-C_6H_5-	p-NO_2	89	221–223	–
5h	Ph	Ph	p-CH_3-C_6H_5-	p-NO_2	88	219–222	219–220[b]
5i	Ph	Ph	p-SO_3H-C_6H_5	p-$N(CH_3)_2$	88	109–112	–
5j	Ph	Ph	–	p-$N(CH_3)_2$	84	255–257	256–259[d]
5k	Ph	Ph	Fu-CH_2	4-OH, 3-CH_3O	87	244–245	–
5l	Fu	Fu	–	4-OH, 3-CH_3O	83	189–190	–
5m	Fu	Fu	–	C_6H_5	82	196–198	197–198[e]
5n	Fu	Fu	Fu-CH_2	p-OH-C_6H_5	89	155–158	–

[a] Indicated yields refer to isolated products

[b] Kantevari et al. (2006)

[c] Khalafi-Nezhad et al. (2016)

[d] Eidi et al. (2016)

[e] Kang et al. (2011)

DMSO-d_6) δ ppm 153.04, 141.33, 137.20, 137.36, 133,58, 131.12, 130.43, 129.7, 129.10, 127.49, 126.94, 126.18, 125.67, 125.26 (C_{arom}), 47.73 (CH_2). **Mass spectrum (ES+)**. 387.18 $[M+H]^+$ 297.13.

(**5d**) 1-benzyl-2-(4-methoxyphenyl)-4,5-diphenyl-1H-imidazole. **MW**: 416.52 **mp**: 165–168 °C (Reported: 167–169 (Khalafi-Nezhad et al. 2016)). **^{1}H-NMR** (600 MHz, DMSO-d_6): δ_H ppm 6,75–8.01 (m, 17H, Ar-H), 5.65 (s, 2H, CH_2), 3.81 (s, 3H, OCH_3). **^{13}C-NMR** (150 MHz, DMSO-d_6): 159.66, 153.70, 147.20, 141.30, 138.82, 137.49, 134.30, 130.70, 129.80, 129.60, 128.59, 127.66, 125.63, 123.20, 114.15(C_{arom}), 55.26(CH_3), 47.66(CH_2). **Mass spectrum (ES+)**. 417.19 $[M+H]^+$ 327.14, 221.14.

(**5e**) 2-(3-nitrophenyl)-4,5-diphenyl-1-(m-tolyl)-1H-imidazole. **MW**: 431.50 **mp**: 165–166 °C (Reported: none reported found). **^{1}H-NMR** (600 MHz, DMSO-d_6): δ_H ppm 7.10–8.80 (m, 18H, Ar-H), 2,35 (s, 3H, CH_3). **^{13}C-NMR** (150 MHz, DMSO-d_6): 149.80, 148.73, 146.04, 145.00, 143.97, 139.15, 138.12, 136.04, 134.86, 132.72, 131.00, 130.08, 129.99, 129.57, 127.83, 126.07, 123.16, 122.19, 118.82, 115.25(C_{arom}), 21.4 (CH_3). **IR (KBr)**: υ_{max}3058(C=C_{arom}), 169(C=N), 1575(N-O), 1460 y 1502(C=C_{arom}), 1335 (C-NO_2). δ_{max} 853(C-$N_{Ar\text{-}NO2}$), 710 y 810(C-$H_{m\text{-}sust}$) cm^{-1}. **Mass spectrum (ES+)**. 432.17 $[M+H]^+$ 418.19, 342.12, 297.13, 221.13, 179.08.

(**5f**) 2-(4-nitrophenyl)-4,5-diphenyl-1-(o-tolyl)-1H-imidazole. **MW**: 431.50 **mp**: 235–236 °C (Reported: none reported found). **^{1}H-NMR** (600 MHz, DMSO-d_6): δ_H ppm 7.12–8.69 (m, 18H, Ar-H), 2.33 (s, 3H, CH_3). **^{13}C-NMR** (150 MHz, DMSO-d_6): 149.63, 148.89, 144.32, 141.74, 137,36, 135.60, 132.30, 131.72, 130.36, 129.65, 129.53, 127.68, 126.93, 126.65, 124.10, 122.36, 117.76(C_{arom}), 17.57(CH_3). **IR (KBr)**: υ_{max}3080(C=C_{arom}), 1685(C=N), 1580(N-O), 1500(C=C_{arom}), 1345(C-NO_2). δ_{max} 860(C-$N_{Ar\text{-}NO2}$), 740(C-$H_{o\text{-}sust}$) cm^{-1}. **Mass spectrum (ES+)**. 432.17 $[M+H]^+$ 387.18, 342.12, 297.14.

(**5g**) 2-(4-nitrophenyl)-4,5-diphenyl-1-(m-tolyl)-1H-imidazole. **MW**: 431.50 **mp**: 221–223 °C (Reported: none reported found). **^{1}H-NMR** (600 MHz, MeOH-d_4): δ_H ppm 7.33–8.31 (m, 12H, Ar-H), 2.21 (s, 3H, CH_3). **^{13}C-NMR** (150 MHz, DMSO-d_6): 149.63, 148.89, 144.32, 141.74, 137,36, 135.60, 132.30, 131.72, 130.36, 129.65, 129.53, 127.68, 126.93, 126.65, 124.10, 122.36, 117.76(C_{arom}), 17.57(CH_3). **IR (KBr)**: υ_{max} 3058 (C=C_{arom}), 1650 (C=N), 1599 (C=C_{arom}), 1335 (C-NO_2), 853 (C-$N_{Ar\text{-}NO2}$), 767 (C-$H_{m\text{-}sust}$) cm^{-1}. **Mass spectrum (ES+)**. 432.17 $[M+H]^+$ 342.12, 179.09, 149.02.

(**5h**) 2-(4-nitrophenyl)-4,5-diphenyl-1-(p-tolyl)-1H-imidazole. **mp**: 219–222 °C (Reported: 219–220 °C (Kantevari et al. 2006)). **MW**: 431.50. **^{1}H-NMR** (600 MHz, MeOH-d_4): δ_H ppm 7.32–8.21 (m, 18H, Ar-H), 2.14 (s, 3H, CH_3). **^{13}C-NMR** (150 MHz, MeOH-d_4): δ_H ppm, 148.81145.56, 139.16, 137.06, 133.29, 130.39, 129.72, 129.61, 129.52, 129.43, 128.92, 128.89, 127.28, 126.82, 125.21, 124.35,

Table 4 Antitrypanosomal, antileishmanial (IC_{50}, μM ± SD), and cytotoxic (MRC-5) (CC_{50}, μM ± SD) activities of arylsubstituted imidazoles. Biological experiments were performed in duplicate

Products	MRC-5	*T.b. brucei*	*T.b. rhod.*	*T. cruzi*	*L. infantum*
5a	1.56 ± 0.2	3.59 ± 0.41	0.86 ± 0.06	1.09 ± 0.01	1.02 ± 0.02
5b	> 64.0	39.85 ± 5.13	37.11 ± 3.88	35.12 ± 5.88	> 64.0
5c	38.62 ± 5.33	3.36 ± 0.34	3.77 ± 0.29	4.07 ± 0.51	10.23 ± 1.16
5d	> 64.0	35.21 ± 7.21	44.11 ± 4.99	34.13 ± 4.87	> 64.0
5e	2.29 ± 0.31	2.11 ± 0.11	2.24 ± 0.31	2.07 ± 0.24	2.07 ± 0.21
5f	2.03 ± 0.14	4.21 ± 0.29	5.17 ± 0.56	1.93 ± 0.23	8.20 ± 0.81
5g	1.12 ± 0.06	2.29 ± 0.21	3.19 ± 0.31	1.80 ± 0.43	1.99 ± 0.19
5h	51.09 ± 4.76	72.22 ± 9.15	14.56 ± 2.67	17.66 ± 3.2	40.89 ± 6.21
5i	4.66 ± 0.32	3.75 ± 0.33	3.29 ± 0.33	4.31 ± 0.51	4.11 ± 0.51
5j	4.11 ± 0.42	4.37 ± 0.43	4.37 ± 0.44	0.96 ± 0.03	4.07 ± 0.42
5k	3.67 ± 0.12	12.33 ± 2.34	12.09 ± 1.33	3.78 ± 0.02	16.44 ± 1.77
5l	13.22 ± 1.22	32.00 ± 4.12	11.99 ± 1.87	18.19 ± 0.20	64.99 ± 8.81
5m	14.67 ± 1.11	35.11 ± 5.89	15.53 ± 2.19	16.99 ± 1.77	48.23 ± 5.51
5n	3.23 ± 0.33	16.23 ± 1.78	24.89 ± 4.12	3.81 ± 0.45	25.47 ± 2.45
Tamoxifen	10.2 ± 1.44				
Suramin		0.03 ± 0.01	0.04 ± 0.01		
Benznidazole				2.89 ± 0.56	
Miltefosine					10.07 ± 4.23

T. cruzi, *Trypanosoma cruzi*; *L. infantum*, *Leishmania infantum*; *T.b. brucei*, *Trypanosoma b. brucei*; *T.b. rhod.*, *Trypanosoma b. rhodesiense*; *MRC-5*, human fetal lung fibroblast cell line

(C_{arom}). 22.15(CH_3). **IR (KBr)**: υ_{max} 3050 (C=C_{arom}), 1615 (C=N), 1500 (C=C_{arom}), 1338 (C-NO_2), δ_{max} 860 (C-$N_{Ar\text{-}NO2}$), 840 (C-$H_{p\text{-}sust}$) cm^{-1}. **Mass spectrum (ES+)**. 432.17 $[M+H]^+$ 342.12, 301.14, 179.09, 149.02, 137.08.

(**5i**) 4-(2-(4-(dimethylamino)phenyl)-4,5-diphenyl-1H-imidazol-1-yl)benzenesulfonic acid. **MW**: 495.60 **mp**: 109–112 °C (Reported: none reported found). **^{1}H-NMR** (600 MHz, DMSO-d_6): δ_H ppm 9.66 (s, 1H, OH), 6.47–7.97(m, 18H, Ar-H), 2.99 (s, 6H, $CH_3 \times 2$). **^{13}C-NMR** (150 MHz, DMSO-d_6): 151.35, 145.87, 143.10, 139.60, 136.40, 130.69, 130.09, 128.72, 128.53, 128.31, 127.40, 126.88, 126.3, 126.21, 113.93, 112.49 (C_{arom}), 40.01 (CH_3x2) ppm. **Mass spectrum (ES−)**. 495.14 $[M-H]^-$, 338.17, 214.01, 172, 155.

(**5j**) 4-(4,5-diphenyl-1H-imidazol-2-yl)-N,N-dimethylaniline. **MW**: 339.44 **mp**: 255–257 °C (Reported: 256–259 °C (Eidi et al. 2016)). **^{1}H-NMR** (600 MHz, DMSO-d_6): δ_H ppm 12.36 (s, 1H, NH), 6.80–7.97 (m, 14H,

Table 5 Selectivity index (SI) of the arylsubstituted imidazole from *T. cruzi*, *L. infantum*, *T.b. brucei*, and *T.b. rhodesiense*

Products	MRC-5/*T.b. brucei*	MRC-5/*T.b. rhod.*	MRC-5/*T. cruzi*	MRC-5/*L. infantum*
5a	0.43	1.81	1.43	1.53
5b	> 1.61	> 1.72	> 1.82	> 1
5c	11.5	10.2	9.49	3.78
5d	> 1.81	> 1.45	> 1.87	> 1
5e	1.09	1.02	1.11	1.11
5f	0.48	0.39	1.05	0.24
5g	0.49	0.35	0.62	0.56
5h	0.71	3.50	2.89	1.25
5i	1.24	1.42	1.08	1.13
5j	0.94	0.94	4.28	1
5k	0.29	0.30	0.97	0.22
5l	0.41	1.10	0.73	0.20
5m	0.42	0.94	0.86	0.30
5n	0.20	0.13	0.85	0.13

Table 6 Binding energy and inhibition constant of the arylsubstituted imidazoles and control CYP51 inhibitors **VNF**, **KET**, and **VFV**

Test comp.	*CYP51—T. cruzi*		*CYP51—L. infantum*		*CYP51—T. brucei*	
	ΔG (kcal/mol)	Ki (nM)	ΔG (kcal/mol)	Ki (nM)	ΔG (kcal/mol)	Ki (nM)
5a	− 9.91	54.32	− 11.13	7.00	− 10.58	17.68
5b	− 9.98	48.54	− 10.37	25.10	− 9.84	61.38
5c	− 9.61	90.61	− 10.74	13.31	− 9.76	69.82
5d	− 10.41	23.31	− 10.95	9.46	− 9.97	49.08
5e	− 13.32	0.17	− 12.88	0.36	− 14.47	0.02
5f	− 13.63	0.10	− 9.22	175.52	− 14.75	0.02
5g	− 13.80	0.08	− 9.40	128.58	− 14.01	0.05
5h	− 13.49	0.13	− 8.44	649.09	− 12.56	0.62
5i	− 14.54	0.02	− 6.39	20,800	− 10.58	17.55
5j	− 9.48	112.65	− 9.84	61.34	− 8.68	437.39
5k	− 9.25	167.21	− 10.61	16.18	− 10.15	36.02
5l	− 7.24	4950	− 7.75	2080	− 8.43	665.25
5m	− 7.31	4370	− 8.19	1000	− 9.07	226.01
5n	− 9.59	93.98	− 10.26	29.97	− 9.83	62.73
VNF	− 9.65	85.03	–	–	–	–
VFV	–	–	− 10.29	28.60	–	–
KET	–	–	–	–	− 11.37	4.60

Ar-H), 2.99 (s, 6H, CH_3x2). **^{13}C-NMR** (150 MHz, DMSO-d_6): δ_H ppm 154.21, 150.36, 146.80, 128.44, 127.84, 126.56, 118.60, 112.03, 111.11(C_{arom}), 43.45 (CH_3x2). **Mass spectrum (ES+)**. 340.18 $[M + H]^+$, 297.14.

(**5k**) 4-(1-(furan-2-ylmethyl)-4,5-diphenyl-1H-imidazol-2-yl)-2-methoxyphenol. **MW**: 422.48 **mp**: 244–245 °C (Reported: none reported found). **^{1}H-NMR** (600 MHz, DMSO-d_6): δ_H ppm 9.28 (s, 1H, OH), 6.85–7.72 (m, 16H, Ar-H, Furanyl), 4.46 (s, 2H, CH_2), 3.83 (s, 3H, CH_3). **^{13}C-NMR** (150 MHz, DMSO-d_6): δ_H ppm 148.72, 147.77, 147.22, 146.08, 142.06, 138.62, 128.50, 128.74, 127.82, 127.52, 127.15, 121.77, 118.52, 115.70, 112.08, 110.92,

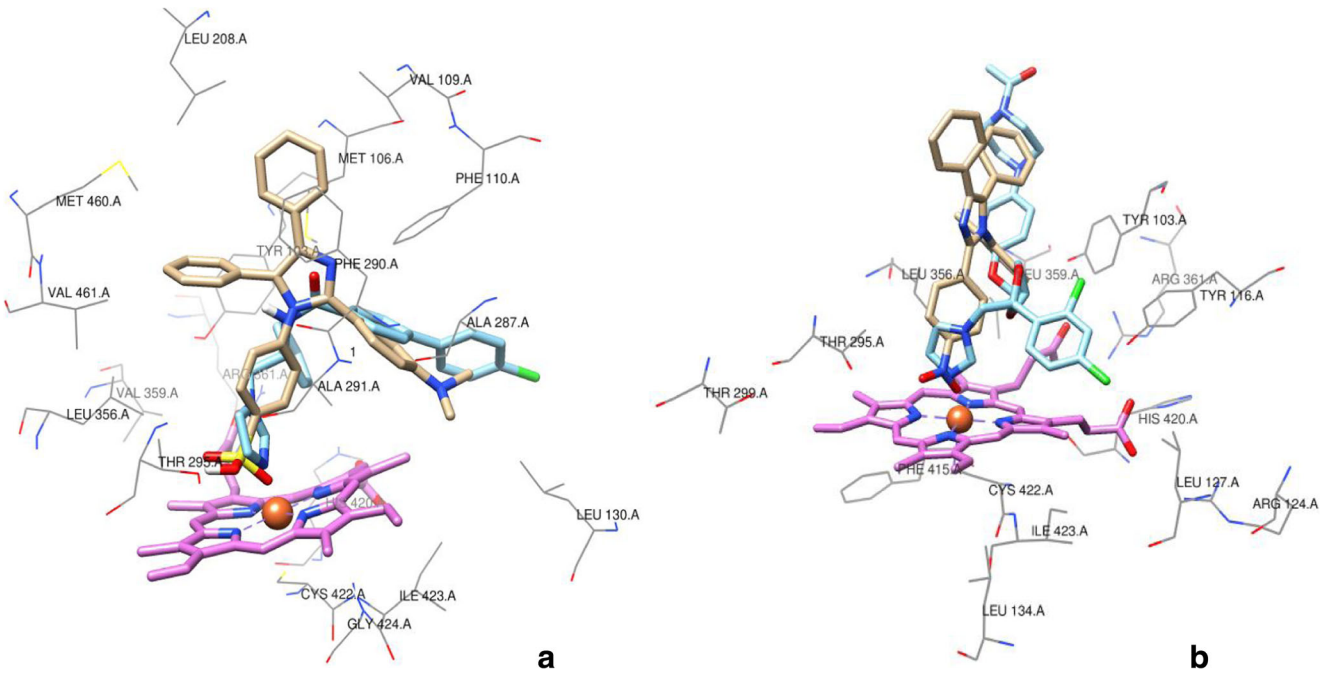

Fig. 3 Superimposition of the best poses of the ligand + control drugs for *CYP51—T. cruzi* in **a 5i** (tan) + **VNF** (sky blue) and **b 5f** (tan) + **KET** (sky blue) for *CYP51—T. brucei* included in the binding pocket

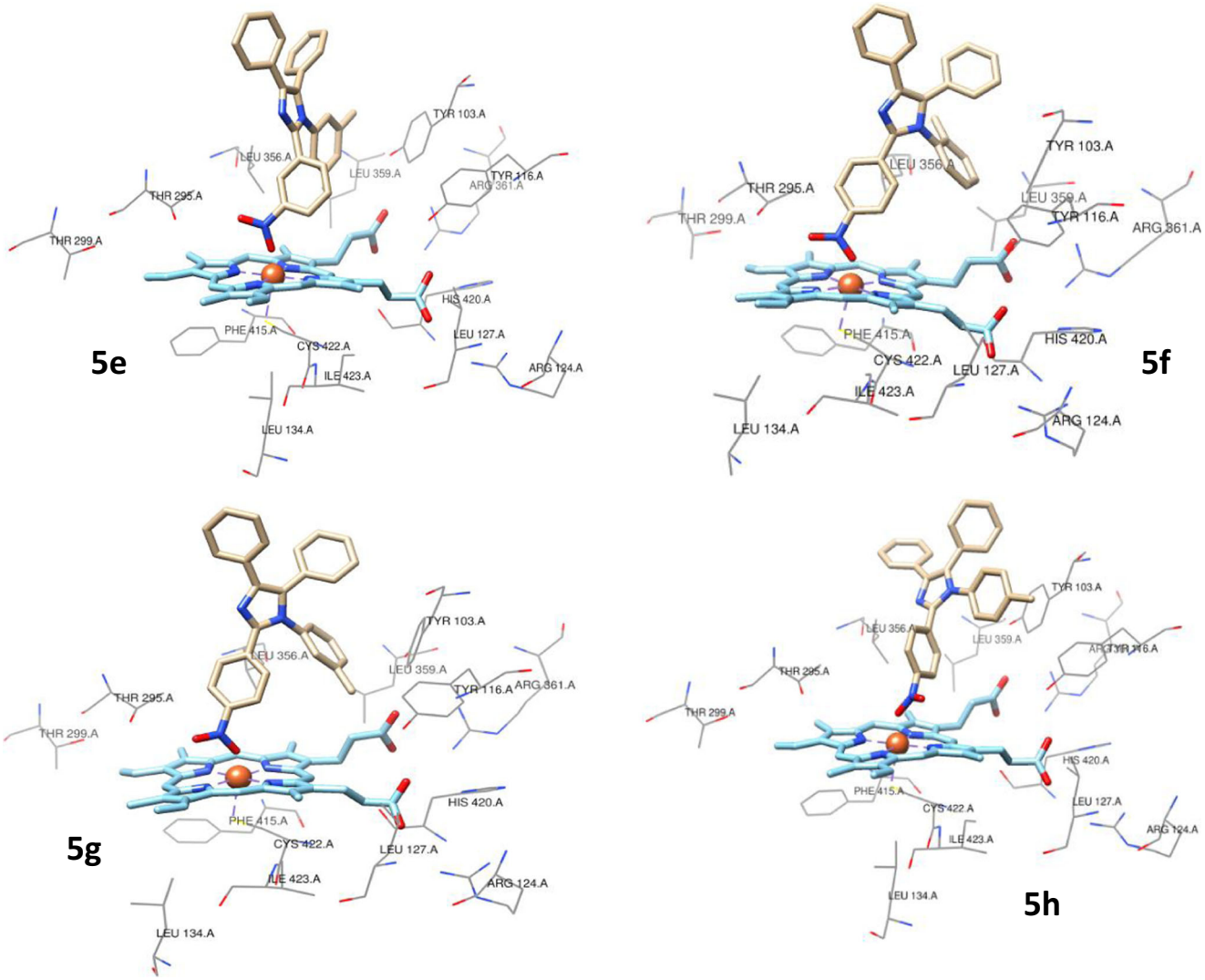

Fig. 4 Similar interaction between ligands **5e**, **5f**, **5g**, and **5h** with the enzyme *CYP51—T. brucei*

105.42, 109.46(C_{arom}), 55.79 (CH_3), 40.01 (CH_2). **Mass spectrum (ES+)**. 423.17 $[M + H]^+$, 343.14, 297.14.

(**5l**) 4-(4,5-di(furan-2-yl)-1H-imidazol-2-yl)-3-methoxyphenol. **MW**: 276.30 **mp**: 189–190 °C (Reported: none reported found). **^{1}H-NMR** (600 MHz, DMSO-d_6): δ_H ppm 3.87 (s, 3H, CH3), 9.33 (s, 1H, OH), 6.57–7.81 (m, 9H, Ar-H, Furanyl), 12.62 (s, 1H, NH). **^{13}C-NMR** (150 MHz, DMSO-d_6): δ_H ppm 144.71, 142.46, 141.80, 129.33, 128.97, 121.29, 120.91, 118.91, 115.67, 112.81, 111.45, 108.18, 106.79(C_{arom}), 55.84(CH_3). **Mass spectrum (ES+)**. 323.10 $[M + H]^+$, 293.09, 201.08.

(**5 m**) 4,5-di(furan-2-yl)-2-phenyl-1H-imidazole. **MW**: 276.30 **mp**: 196–198 (Reported: 197–198 °C (Kang et al. 2011)). **^{1}H-NMR** (600 MHz, DMSO-d_6): δ_H ppm 6.58–8.10 (m, 11H, Ar-H, Furanyl), 12.87 (s, 1H, NH). **^{13}C-NMR** (150 MHz, DMSO-d_6): δ_H ppm 149.34, 146.32, 144.48, 142.69, 141.94, 129.89, 128.78, 119.42, 111.96, 106.98(C_{arom}). **Mass spectrum (ES+)**. 277.09 $[M + H]^+$, 201.07.

(**5n**) 4-(4,5-di(furan-2-yl)-1-(furan-2-ylmethyl)-1H-imidazol-2-yl)phenol. **MW**: 392.46 **mp**: 155–158 (Reported: none reported found). **^{1}H-NMR** (600 MHz, DMSO-d_6): δ_H ppm 9.79 (s, 1H, Ar-OH), 3.42 (s, 2H, CH_2), 6.87–7.92 (m, 13H, Ar-H, Furanyl). **^{13}C-NMR** (150 MHz, DMSO-d_6): δ_H ppm 158.50, 157.91, 153.67, 151.30, 146.19, 142.9, 142.1, 130.75, 128.48, 127.80, 126.98, 121.73, 115.96, 107.70(C_{arom}), 37.80 (CH_2). **Mass spectrum (ES+)**. 373.12 $[M + H]^+$ 293.09, 277.10.

Antiprotozoal and cytotoxic effects

The antiparasitic activities and the cytotoxicity of the test and reference compounds are listed in Table 4. All compounds were tested in vitro against the tripomastigotes stage of *T.b. brucei* and *T.b. rhodesiense* and amastigote stage of *T. cruzi* and *L. infantum*. The cytotoxicity of all arylsubstituted imidazoles against MRC-5 cell lines (human lung fibroblasts) was evaluated and the

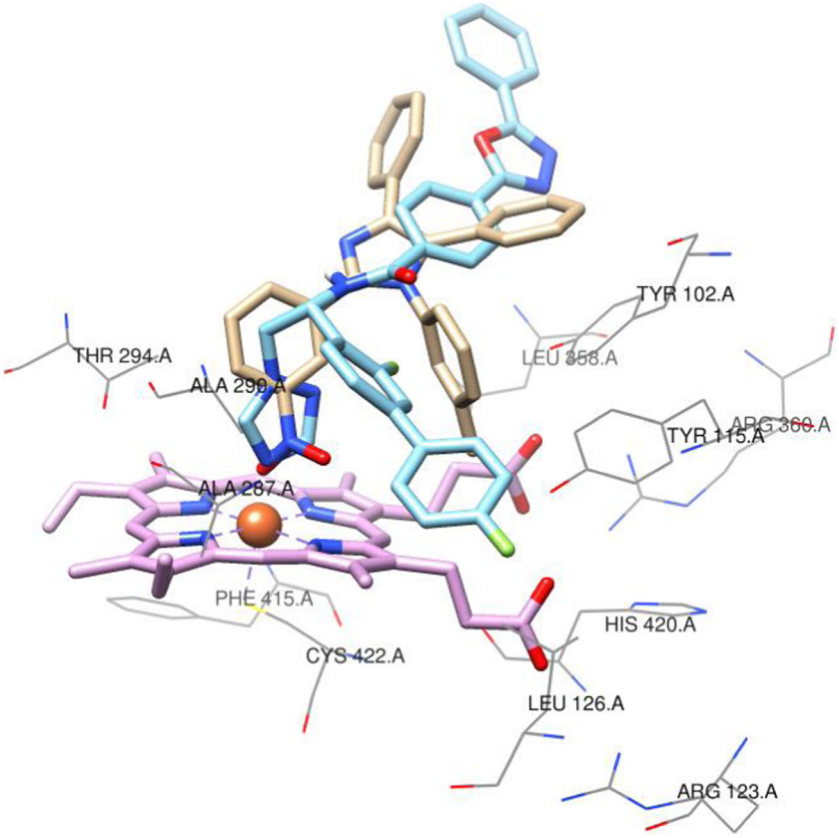

Fig. 5 Superimposition of the best pose of the **5e** (tan) + **VFV** (sky blue) included in the binding pocket of *CYP51—L. infantum*

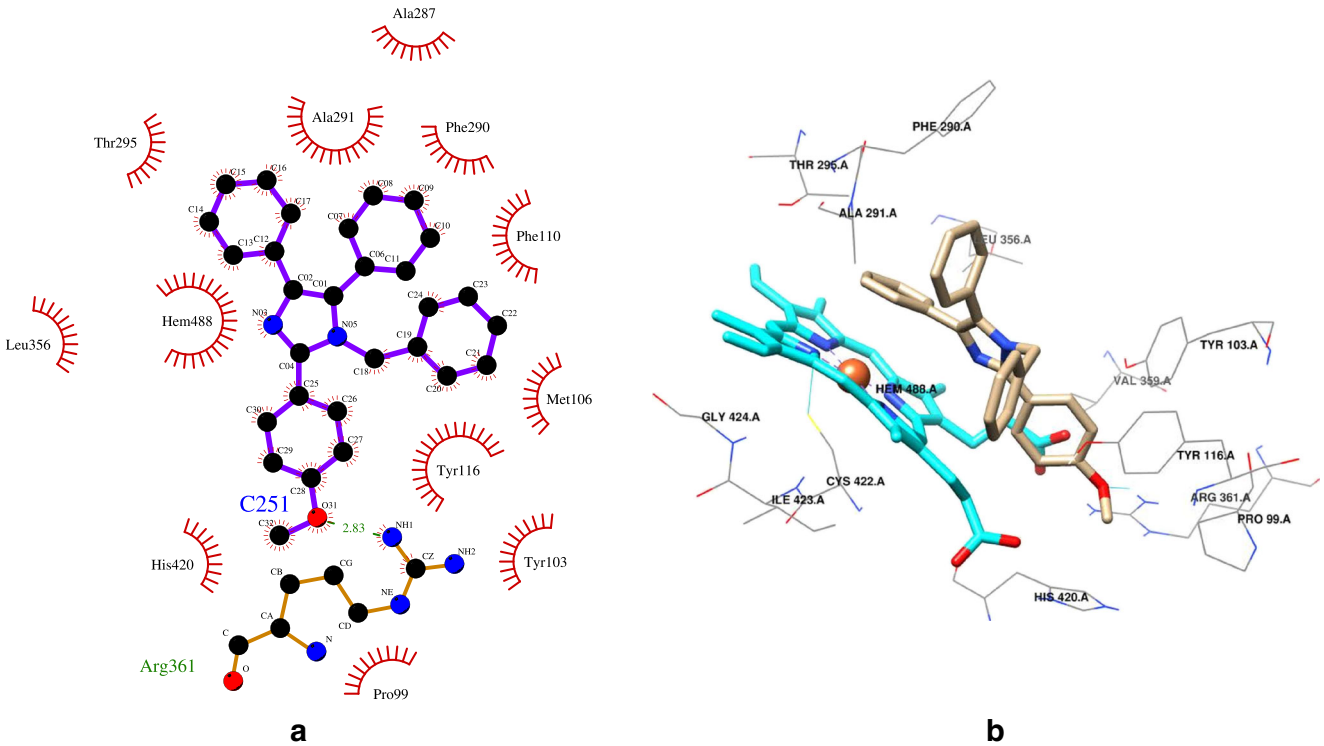

Fig. 6 Docked structures of compound **5d** in *CYP51—T. cruzi*; **a** two-dimensional representations of interaction by the Ligplot software (Wallace et al. 1996); **b** three-dimensional representation of the interaction the ligand (tan) and Heme group (cyan)

selectivity indices (SI) (SI = CC_{50} MRC-5 cells/IC_{50} protozoa) were calculated (Table 5) (Ehata et al. 2012).

The imidazoles **5a**, **5c**, **5e**, **5f**, **5g**, **5i**, **5j**, **5k**, and **5n** exhibited IC_{50} values lower than 5 μM against *T. cruzi*. The ligands **5l**, **5m**, and **5h** had a moderate activity with IC_{50} values of 18.19, 16.99, and 17.66 μM, respectively. Only the ligands **5d** and **5b**, both with similar structure (Table 1) substituted in position two of the arylsubstituted imidazole by a hydroxyl (OH) and a methoxy (OCH_3), showed a low activity. The most active compounds **5a**, **5f**, **5g**, and **5j** showed lower IC_{50} values than the reference compound benznidazole (Table 4). However, only compound **5c** with an IC_{50} of 4.07 μM presented a good selectivity towards *T. cruzi* with a SI of 9.49 (Table 5).

On the other hand, against *T.b. brucei* and *T.b. rhodesiense*, the active compounds were **5a**, **5c**, **5e**, **5f**, **5g**, **5i**, and **5j**. The most active compound against *T.b. brucei* was **5e** (IC_{50} = 2.11 μM), while for *T.b. rhodesiense* the most active compound was **5a** with an IC_{50} = 0.86 μM. Both compounds were less active than the reference compounds **suramin** for *T.b. brucei* (0.03 μM) and *T.b. rhodesiense* (0.04 μM). For *T.b. rhodesiense*, the ligands with a good activity were **5h**, **5k**, **5l**, and **5m**, with IC_{50} values between 11.99 and 15.53 μM. Ligands **5k** and **5l** have a similar structure in position two of the imidazoles with a phenyl group joined to a hydroxyl (4-OH) substituent and a methoxyl (3-CH_3O) group.

None of studied arylsubstituted imidazoles showed a higher activity than the reference drug suramin towards *T.b. rhodesiense*, demonstrating the lower sensitivity for this class of compounds (De Vita et al. 2016). Only the ligand **5a** (IC_{50} = 0.86 μM) possessed an IC_{50} value comparable with the control drug **suramin**.

Compounds **5a**, **5c**, **5e**, **5f**, **5g**, **5i**, and **5j** presented similar antileishmanial activity compared with the control drug **miltefosine**, but they showed a pronounced cytotoxicity on MRC-5 cells (Table 4), indicating the lack of selectivity towards *L. infantum* (Table 5).

Compound **5c** had the highest selectivity to the Trypanosoma family with a SI of 9.49, 11.5, and 10.2 for *T. cruzi*, *T.b. brucei*, and *T.b. rhodesiense*, respectively (Table 5).

Molecular docking

The procedure adopted for the molecular docking was used for all designed arylsubstituted imidazoles (Table 1) with each

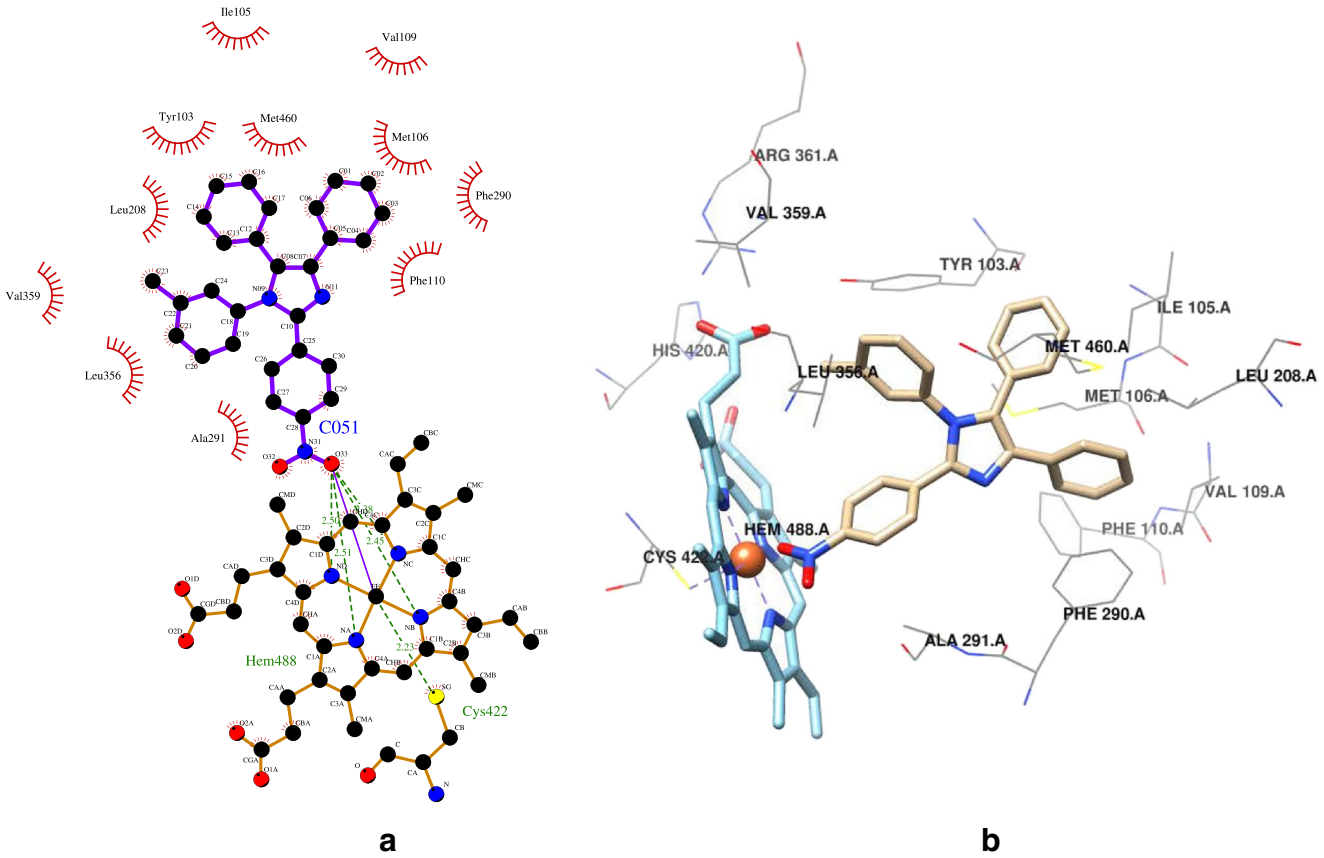

Fig. 7 Docked structures of compound **5g** in the *CYP51—T. cruzi*; **a** 2D interaction by the Ligplot software; **b** 3D representation of the interaction the ligand (tan) and the heme group (cyan)

target selected. The docked poses for each of the compounds have been evaluated and the pose with the lowest binding free energy and inhibition constant was thereby chosen (Table 6).

The lowest binding free energy (i.e., best docking score) and inhibition constant indicates the highest ligand/protein affinity. The docking studies were done in comparison with control drugs (i.e., known inhibitors of the target enzymes). The control drugs were redocked with each protein target chosen, **VNF** for *CYP51—T. cruzi*, **VFV** for *CYP51—L. infantum*, and **KET** for *CYP51—T. brucei*.

As shown in Table 6, the binding energies (ΔG) and inhibition constant (Ki) of the control drug **VNF** in the docking with *CYP51—T. cruzi* were found to be − 9.65 kcal/mol and 85.03 nM, respectively. However, the value for almost designed imidazoles was found to be higher than the **VNF** control, with ΔG value between − 9.25 and − 14.54 kcal/mol and low values of Ki. The ligand **5i** shows the better values (ΔG = − 14.54 kcal/mol and Ki = 0.02 nM) and a similar conformation compared with the **VNF** control (Fig. 3a), other ligands showed better values and only the ligands **5l** and **5m** showed not accepted values of binding energies and inhibition constant compared with the control.

In the case of *CYP51—T. brucei*, the binding energy (ΔG) of the control drug ketoconazole was − 11.37 kcal/mol (Ki = 4.60 nM), exceeded only by the ligands **5e**, **5f**, **5g**, and **5h** with a binding energy of − 14.47, − 14.75, − 14.01, and − 12.56 kcal/mol, respectively, and Ki values very low compared with the **KET** control. The best ligand **5f** showed similar conformation respect to **KET** control (Fig. 3b) and the ligands **5e**, **5g**, and **5h** presented similar values (ΔG and Ki) to ligand **5f**, due to the same interaction with the Heme group through the oxygen presented in the NO_2 group (Fig. 4).

For enzyme *CYP51—L. infantum* with the control drug **VFV**, the binding energy was found to be − 10.29 kcal/mol with a Ki = 28.60 nM. The values of **VFV** are only exceeded by ligands **5a**, **5b**, **5c**, **5d**, **5e**, **5k** were found to have − 11.13, − 10.37, − 10.74, − 10.95, − 12.88, and − 10.61, respectively, for the binding energy and Ki values very low respect to the **VFV** control (Table 6). The best ligand was **5e** and we can observe in Fig. 5 the superimposition between **VFV** and **5e**, where both ligands interacted directly with the Heme group.

It should be noted that ligand **5e** appeared to bind in the three receptor enzymes (*CYP51—T. cruzi*, *CYP51—L. infantum*, *CYP51—T. brucei*) and in all cases this ligand had lower ΔG values when compared to the control drugs. Some similar behavior occurs with the ligands **5a** and **5k** binding to *CYP51—L. infantum* and *CYP51—T. brucei* and **5f**, **5g**, **5h**, and **5i** binding with *CYP51—T. cruzi* and *CYP51—T. brucei*. All of them show better binding values than the control drugs. Our molecular docking studies revealed that all compounds (**5a–n**) in one way or another interacted with the 14 α-

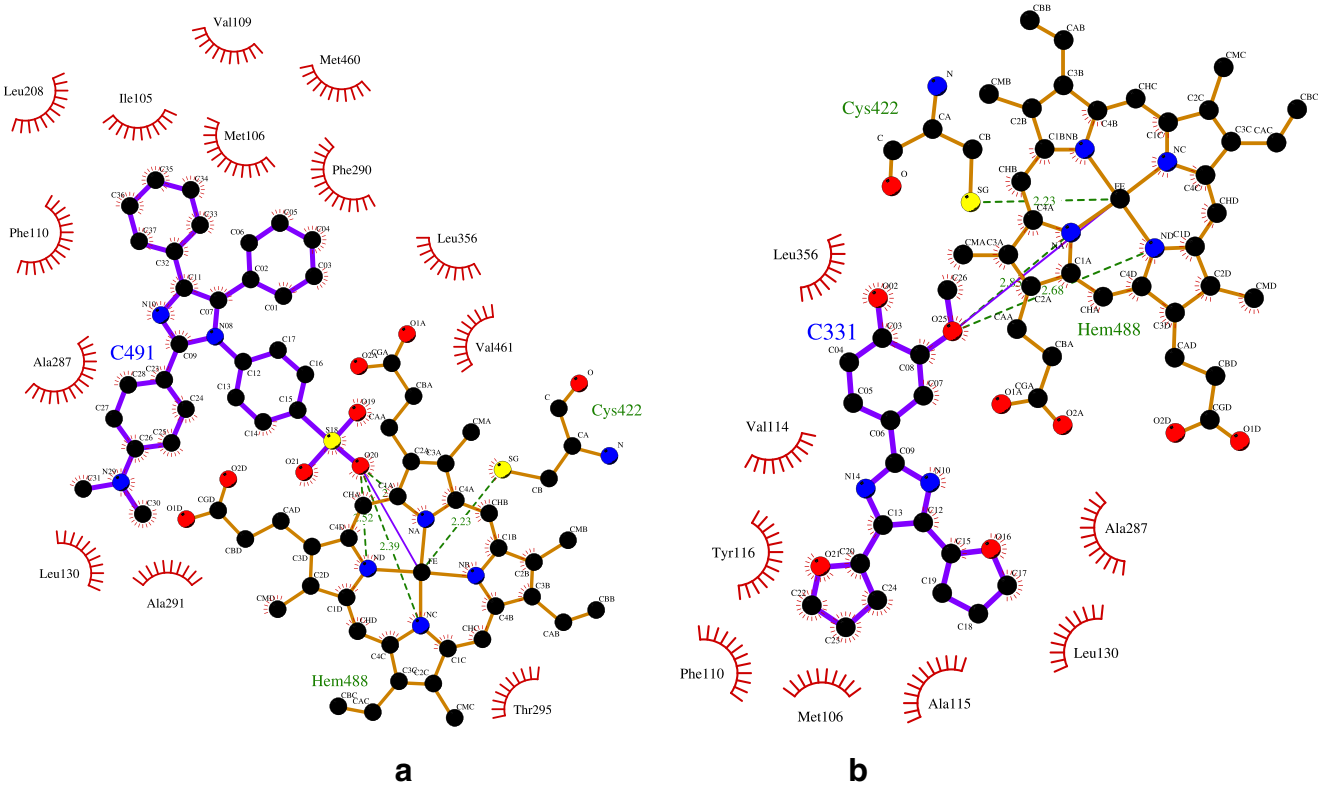

Fig. 8 Docked structures of compounds **5i** (**a**) and **5l** (**b**) in the *CYP51—T. cruzi* pocket represented using the Ligplot software

demethylase enzyme for each species (*CYP51—T. cruzi*, *CYP51—L. infantum*, *CYP51—T. brucei*) by hydrophobic interactions or azole-Heme coordination and π-π and π-cation interactions.

This study with *CYP51—T. cruzi* demonstrated that in some ligands (**5a**, **5b**, **5c**, **5d**, **5j**, **5k**, **5m**, and **5n**) there are hydrophobic interactions with the Heme group (Fig. 6).

We see also hydrogen bond interactions with amino acid residue Arg361 (**5b**, **5d**, and **5n**). All ligands showed hydrophobic interaction with Ala291, Ala287, Phe290, Phe110, Met106, Tyr116, Tyr103, Pro99, His420, Leu356, and Thr295. They shared some residues Ala291, Ala287, Phe290, Phe110, Met106, Tyr116, Tyr103, Leu356, and Thr295 involved in the active site according to Lepesheva et al. (2010). The ligands **5e**, **5f**, **5g**, and **5h** showed an electronic interaction between the NO_2 group (electron pair of oxygen O33) and the Fe^{2+} of Hem488 group (Fig. 7); however for ligand **5i** and **5l**, the interaction with the Hem488 is with SO_3H (electron pair of O20) for **5i** and OCH_3 (electron pair of O25) for **5l** (Fig. 8).

The ligands **5e**, **5f**, **5g**, and **5h** also showed the interaction with the heme group. We could observe the hydrophobic interaction with Ala291, Ala287, Phe290, Phe110, Met106, Tyr116, Tyr103, Pro99, His420, Leu356, and Thr295 similar as seen with the ligands **5a**, **5b**, **5c**, **5d**, **5j**, **5k**, **5m**, and **5n** where they share the same residues involved in the active site.

In the case of *CYP51—L. infantum*, only the ligands **5e** and **5h** showed interaction between one of the NO_2 group's oxygens (O32) with the heme group (Fig. 9a) and in the ligand **5i** complex the interaction was with the SO_3H group's oxygen atoms (Fig. 9b).

On the other hand, the ligands **5a**, **5b**, **5c**, **5d**, **5j**, **5k**, **5l**, **5m**, and **5n** were found to have hydrophobic interactions with Met359, Val212, Pro209, Me459, Val356, Met357, Val460, Thr294, Ala290, Leu355, Phe109, Met105, Phe289, Tyr115, Tyr102, Phe104, and Hem481 (Fig. 10). These ligands share some residues Leu355, Met357, Val212, Phe104, Met105, Tyr115, Phe109, and Ala290 involved in the active site according to Hargrove et al. (2011).

Compounds **5a**, **5b**, **5c**, **5d**, **5i**, **5j**, **5k**, **5l**, and **5m** were found to establish hydrophobic interactions with *CYP51—T. brucei* (Fig. 11) that involved the residues Val461, Ala291, Phe290, Thr295, His294, Phe105, Tyr103, Met106, Tyr116, Leu127,

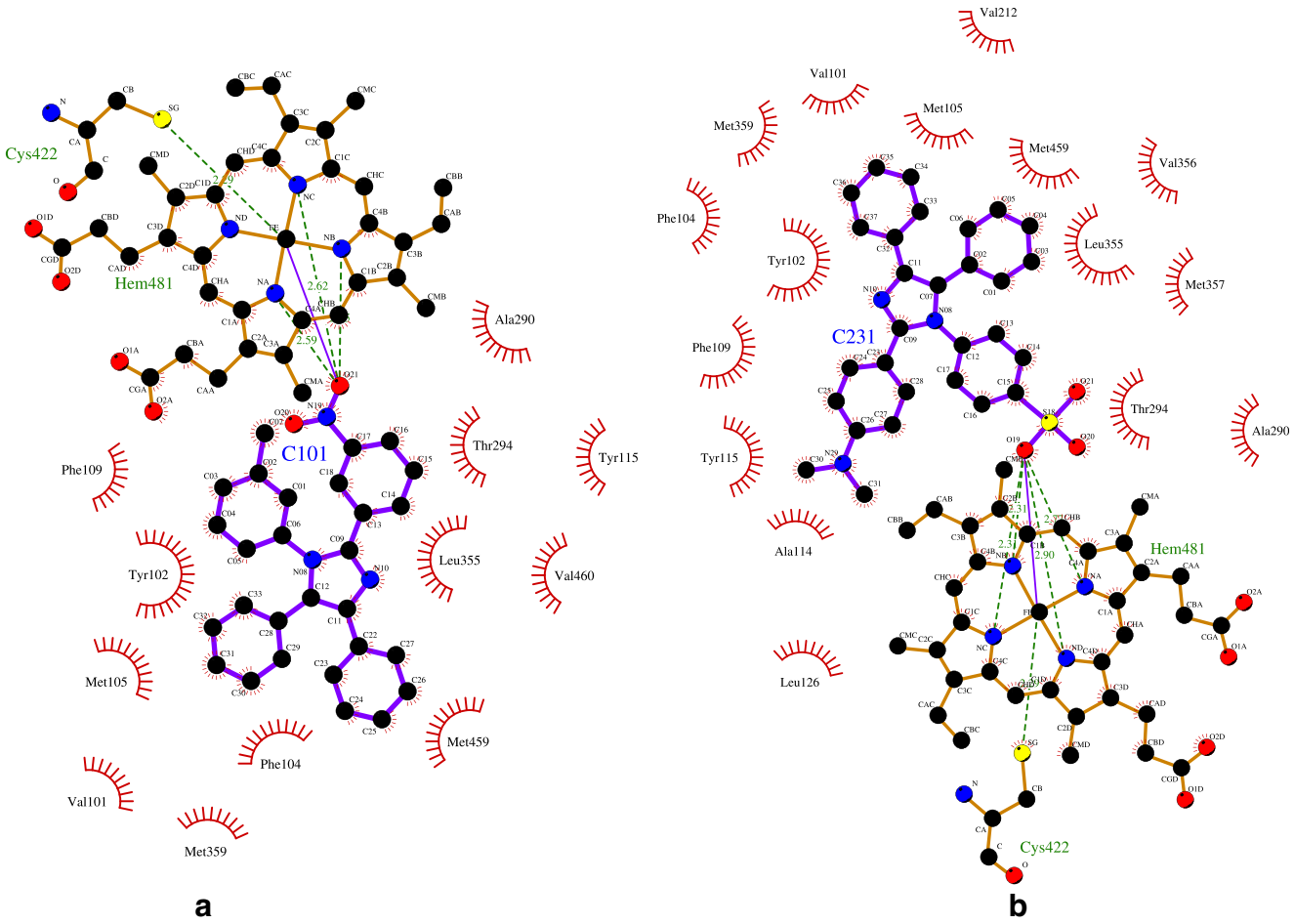

Fig. 9 Docked structures of compounds **5e** (**a**) and **5i** (**b**) in the *CYP51—L. infantum* pocket represented using the Ligplot software

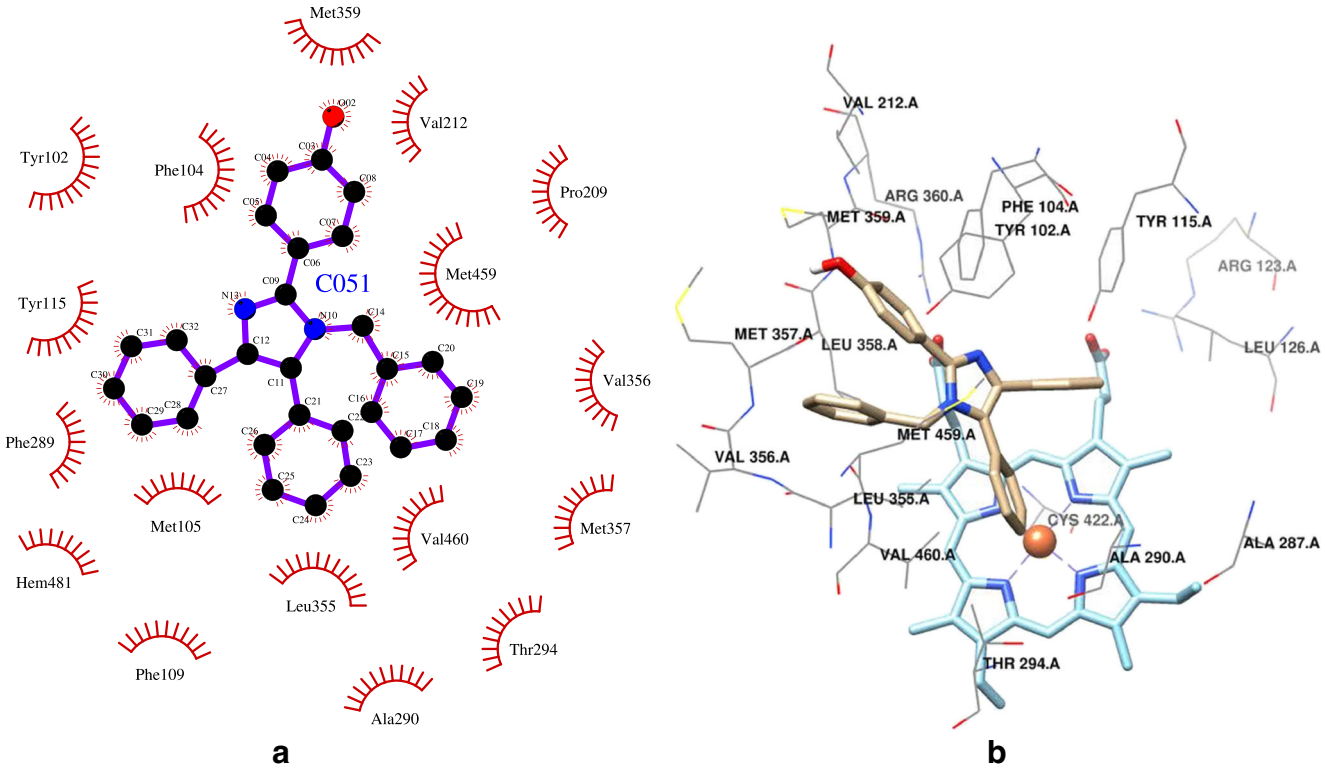

Fig. 10 Docked structures of compound **5b** in the *CYP51—L. infantum*; **a** 2D interaction by Ligplot software, **b** 3D representation of the interaction the ligand (tan) and Heme group (cyan)

Ala115, Ala287, Phe110, Hem1450, and His294. All those compounds (**5a**, **5b**, **5c**, **5d**, **5i**, **5j**, **5k**, **5l**, and **5m**) share some residues: Tyr116, Tyr103, Met106, Phe105, Phe290, Ala287, and Phe110 involved in the active site (Choi et al. 2013).

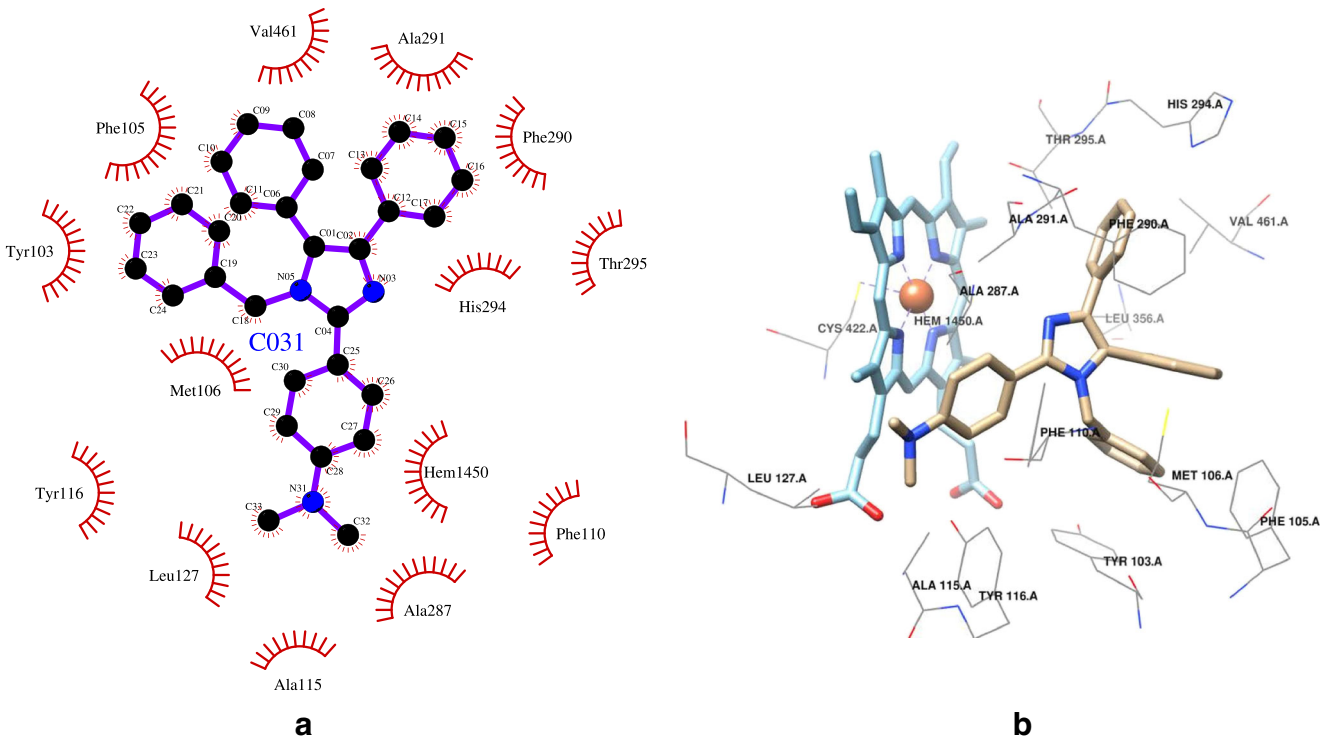

Fig. 11 Docked structures of compound **5a** in the *CYP51—T. brucei*; **a** 2D interaction by Ligplot software, **b** 3D representation of the interaction the ligand (tan) and Heme group (cyan)

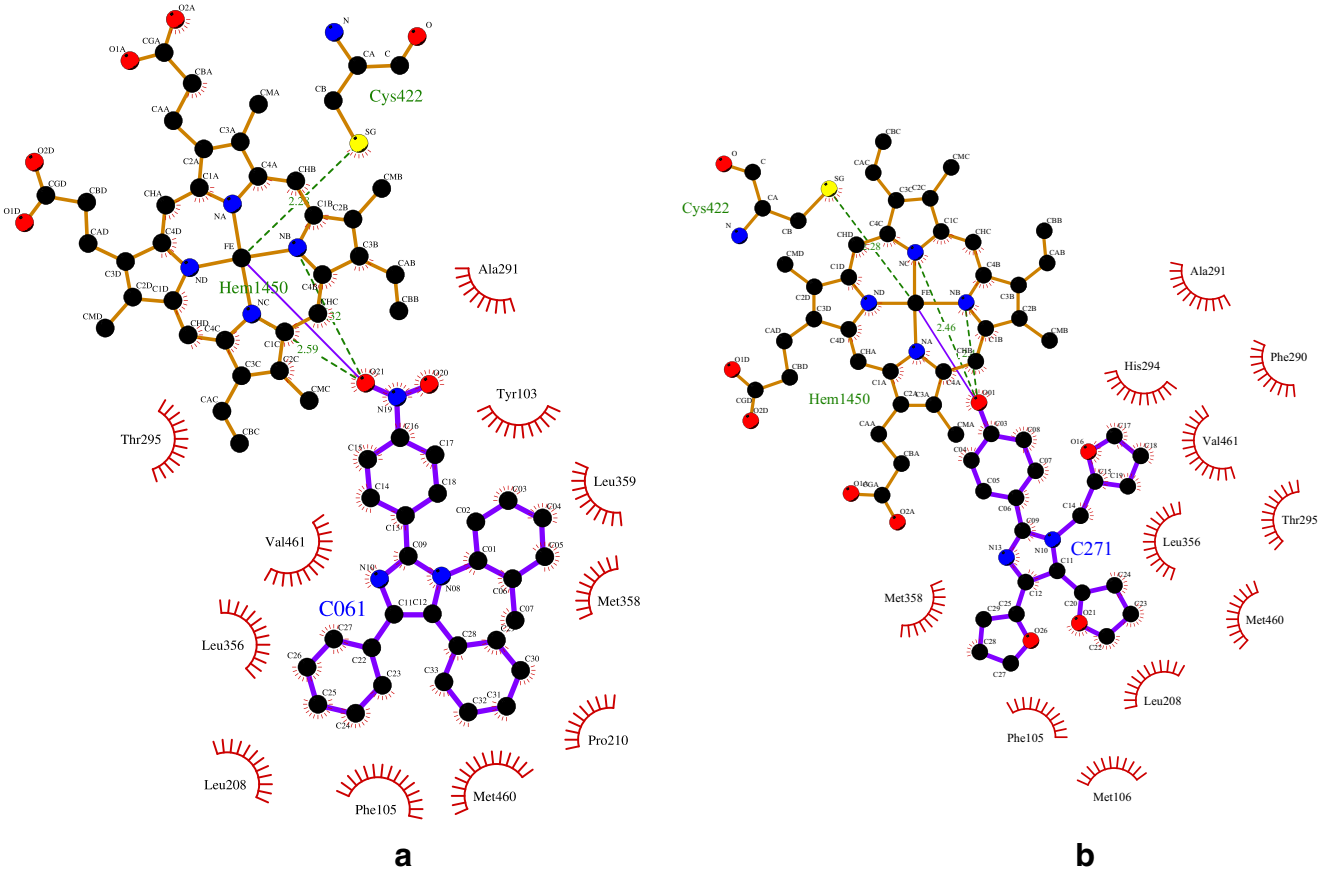

Fig. 12 Docked structures of compounds **5f** (**a**) and **5n** (**b**) in the *CYP51—T. brucei* pocket represented using the Ligplot software

On the other hand, the ligands **5e**, **5f**, **5g**, **5h**, and **5n** were observed to interact with the Heme group through the NO_2 function for **5e**, **5f**, **5g**, **5h** and with OH for **5n** (Fig. 12).

These results reveal that the position of the substituent in the phenyl joined to the imidazole ring in the four positions affected strongly the orientation and the subsequently interaction of the imidazoles with the Heme iron atom in the binding site of the enzyme.

Conclusions

In conclusion, the present investigation has described the chemical synthesis and antiprotozoal, cytotoxic activities of several arylsubstituted imidazoles as well as their molecular docking in the active site of CYP51 of those protozoa. The reported results showed that all samples possessed interesting in vitro antiprotozoal activity at different extents. The ligand **5c** was found to be non-toxic according to the study conducted with the MRC-5 cell line and the best selectivity index against *T. cruzi*, *T.b. brucei*, and *T.b. rhodesiense*. The main interactions, studied by molecular docking, are hydrophobic between the substituents in positions 1, 4, and 5 of the imidazolic rings and residues in the active site. Electrostatic interactions were identified between oxygen fundamentally present in NO_2, SO_3H, and OH groups and the Fe^{2+} ion of the Heme group. The reported results can partly justify and support the possible use of some of these imidazoles for the treatment of parasitic diseases such as sleeping sickness, leishmaniasis, and in some extent American trypanosomiasis named Chagas disease, with no apparent toxic effects in patients.

Acknowledgements This work has been supported by the Belgian Development Cooperation through VLIR-UOS (Flemish Interuniversity Council-University Cooperation for Development) in the context of the Institutional University Cooperation programme with Universidad de Oriente, Santiago de Cuba, Cuba started in 2013.

References

Anusha S, Baburajeev CP, Mohan CD, Mathai J, Rangappa S et al (2015) A nano-MgO and ionic liquid-catalyzed 'green' synthesis protocol for the development of adamntyl-imidazolo-thiadiazoles as antituberculosis agents targeting sterol 14α-demethylase (CYP51). Plosone 10(10):e0139798

Bates PA (2007) Transmission of *Leishmania* metacyclic promastigotes by phlebotomine sand flies. Int J Parasitol 37:1097–1106

Buckner FS, Urbina JA (2012) Recent developments in sterol 14-demethylase inhibitors for Chagas disease. Int J Parasitol-Drug 2: 236–242

Choi JY, Calvet CM, Gunatilleke SS, Ruiz C, Cameron MD, Mckerrow JH, Podust LM, Roush WR (2013) Rational development of 4-aminopyridyl-based inhibitors targeting *Trypanosoma cruzi* CYP51 as anti-Chagas agents. J Med Chem 56:7651–7668

Cos P, Vlietinck AJ, Berghe DV, Maes L (2006) Anti-infective potential of natural products: how to develop a stronger in vitro 'proof-of-concept'. J Ethnopharmacol 106(3):290–302

De Vita D, Moraca F, Zamperini C, Pandolfi F, Di Santo R, Matheeussen A, Maes L, Tortorella S, Scipione L (2016) In vitro screening of 2-(1H-imidazol-1-yl)-1-phenylethanol derivatives as antiprotozoal agents and docking studies on *Trypanosoma cruzi* CYP51. Eur J Med Chem 113:28–33

Ehata MT, Phuati AM, Lumpu SN, Munduki CK, Phongi DB, Lutete GT, Kabangu OK, Kanyanga RC, Matheeussen A, Cos P, Apers S, Pieters L, Maes L, Vlietinck AJ (2012) In vitro antiprotozoal and cytotoxic activity of the aqueous extract, the 80% methanol extract and its fractions from the seeds of *Brucea sumatrana* Roxb. (Simaroubaceae) growing in Democratic Republic of Congo. Chin Med 3:65–71

Eidi E, Kassaee MZ, Nasresfahani Z (2016) Synthesis of 2,4,5-trisubstituted imidazoles over reusable CoFe2O4 nanoparticles: an efficient and green sonochemical process. Appl Organometal Chem 30:561–565

Evans DA (2014) History of the Harvard ChemDraw Project. Angew Chem Int Ed 53:11140–11145

Friggeri L, Hargrove TY, Rachakonda G, Williams AD, Wawrzak Z, Di Santo R, De Vita D, Waterman MR, Tortorella S, Villalta F, Lepesheva GI (2014) Structural basis for rational design of inhibitors targeting *Trypanosoma cruzi* sterol 14α-demethylase: two regions of the enzyme molecule potentiate its inhibition. J Med Chem 57:6704–6717

Gasteiger J, Marsili M (1980) Iterative partial equalization of orbital electronegativity a rapid access to atomic charges. Tetrahedron 36: 3219–3228

Guedes da Silva FH, Batista DGJ, Da Silva CF, De Araújo JS, Pavão BP et al (2017) Anti-trypanosomal activity of sterol 14α-demethylase (CYP51) inhibitors VNI and VFV in the Swiss mouse models of Chagas disease induced by the Y strain *Trypanosoma cruzi*. Antimicrob Agents Chemother 61(4):e02098–e02016

Hargrove TY, Wawrzak Z, Liu J, Nes WD, Waterman MR, Lepesheva GI (2011) Substrate preferences and catalytic parameters determined by structural characteristics of sterol 14alpha-demethylase (CYP51) from *Leishmania infantum*. J Biol Chem 286:26838–26848

Hargrove TY, Kim K, de Nazaré Correia Soeiro M, da Silva CF, Batista DD, Batista MM, Yazlovitskaya EM, Waterman MR, Sulikowski GA, Lepesheva GI (2012) CYP51 structures and structure-based development of novel, pathogen-specific inhibitory scaffolds. Int J Parasitol Drugs Drug Resist 2:178–186

Kang J, Zhang Y, Han L, Tang J, Wang S, Zhang Y (2011) Utilizing the chemiluminescence of 2-substituted-4,5-di(2-furyl)-1H-imidazole–H_2O_2–Cu^{2+} system for the determination of Cu^{2+}. J Photochem Photobiol A Chem 217:376–382

Kantevari S, Vuppalapati SVN, Biradar DO, Nagarapu L (2006) Highly efficient, one-pot, solvent-free synthesis of tetrasubstituted imidazoles using HClO4–SiO_2 as novel heterogeneous catalyst. J Mol Catalysis A: Chem 266:109–113

Khalafi-Nezhad A, Shekouhy M, Sharghi H, Aboonajmi J, Zare A (2016) A new more atom-efficient multi-component approach to tetrasubstituted imidazoles: one-pot condensation of nitriles, amines and benzoin. RSC Adv 6:67281–67289

Lepesheva GI, Hargrove TY, Anderson S, Kleshchenko Y, Furtak V, Wawrzak Z, Villalta F, Waterman MR (2010) Structural insights into inhibition of sterol 14α-demethylase in the human pathogen *Trypanosoma cruzi*. J Biol Chem 285:25582–25590

Lepesheva GI, Hargrove TY, Rachakonda G, Wawrzak Z, Pomel S, Cojean S, Pius NN, Nes WD, Locuson CW, Wade Calcutt M, Waterman MR, Scott Daniels J, Loiseau PM, Villalta F (2015) VFV as a new effective CYP51 structure-derived drug candidate for Chagas disease and visceral leishmaniasis. J Infect Dis 212(9): 1439–1448

Pettersen EF, Goddard TD, Huang CC, Couch GS, Greenblatt DM, Meng EC, Ferrin TE (2004) UCSF chimera—a visualization system for exploratory research and analysis. J Comput Chem 25(13):1605–1612

Planche AS, Scotti MT, López AG, de Paulo Emerenciano V, Pérez EM, Uriarte E (2009) Design of novel antituberculosis compounds using graph-theoretical and substructural approaches. Mol Divers 13:445–458

Roberts CW, McLeod R, Rice DW, Ginger M, Chance ML, Goad LJ (2003) Fatty acid and sterol metabolism: potential antimicrobial targets in apicomplexan and trypanosomatid parasitic protozoa. Mol Biochem Parasit 126:129–142

Rodríguez NE, Gaur U, Wilson ME (2006) Role of caveolae in *Leishmania chagasi* phagocytosis and intracellular survival in macrophages. Cell Microbiol 8:1106–1120

Sanner MF (1999) Python: a programming language for software integration and development. J Mol Graphics Mod 17:57–61

Schel WA, Jones AM, Garvey EP, Hoekstra WJ, Schotzinger RJ (2016) Fungal CYP51 inhibitors VT-1161 and VT-1129 exhibit strong in vitro activity against *Candida glabrata* and *C. krusei* isolates clinically resistant to azole and echinocandin antifungal compounds. Antimicrob Agents Chemother 61(6):e01817-16

Shelke KF, Sapkal SB, Sonar SS, Madje BR, Shingate BB, Shingare MS (2009) An efficient synthesis of 2,4,5-triaryl-1H-imidazole derivatives catalyzed by boric acid in aqueous media under ultrasound-irradiation. Bull Kor Chem Soc 30:1057–1060

Singh A, Paliwal SK, Sharma M, Mittal A, Sharma S (2015) In silico and in vitro screening to identify structurally diverse non-azole CYP51 inhibitors as potent antifungal agent. J Mol Graph Model 63:1–7

Wallace AC, Laskowski RA, Thornton JM (1996) LIGPLOT: a program to generate schematic diagrams of protein-ligand interactions. Protein Eng 8(2):127–134

World Health Organization (2017) http://www.who.int/gho/publications/world_health_statis-tics/2017/en/. Accessed 21 Jan 2018